Heat Transfer Measurements on the Endwall of a Variable Speed Power Turbine Blade Cascade

Douglas Thurman
Aerospace Engineer
Army Research Laboratory
Cleveland, OH, USA

Philip Poinsatte
Aerospace Engineer
NASA Glenn Research Center
Cleveland, OH, USA

Paul Giel
Aerospace Engineer
Vantage Partners
Cleveland, OH, USA

Barbara Lucci
Aerospace Engineer
NASA Glenn Research Center
Cleveland, OH, USA

ABSTRACT

Heat transfer measurements were obtained on the endwall of a 2-D section of a variable speed power turbine (VSPT) rotor blade linear cascade. Infrared thermography was used to help determine the transition of flow from laminar to turbulent as well as determine regions of flow separation. Steady state data was obtained for six incidence angles ranging from +15.8° to -51°, and at five flow conditions for each angle. Nusselt number was used as a method to visualize flow transition and separation on the endwall surface and showed the effects of secondary flows on the surface. Nusselt correlation with Reynolds number from multiple flow conditions was used to plot local values of the correlation exponent and indicated the state of the local boundary layer as the flow transitioned from laminar to turbulent as well as secondary flow features.

NOTATION

C_{pt}	total-pressure coefficient, $C_{pt} = (P_{t,1}–P_t)/(P_{t,1}–P_2)$
C_x	blade axial chord [in]
i	incidence angle, $i = \beta_1$ – inlet metal angle (34.2°)
M	Mach number
PR	pressure ratio, $PR = P_{t,1}/P_2$
PS	pressure surface
P	area-averaged static-pressure
P_t	area-averaged total-pressure
Re	Reynolds number, $Re = \rho U C_x/\mu$
Re_b	baseline Reynolds number, $Re_b = 5.30\times10^5$
S	blade pitch [in]
SS	suction surface
U	total mean velocity
x	chordwise (axial) coordinate [in]
y	pitchwise (tangential) coordinate [in]
z	spanwise coordinate [in]
Zw	Zweifel coefficient, $Zw = \frac{2S}{C_x}\cos^2\beta_2(\tan\beta_1-\tan\beta_2)$
β	relative flow angle, pitch angle [deg], $\beta=\tan^{-1}(U_y/U_x)$
μ	dynamic viscosity
ρ	density

Subscripts

1	cascade inlet value
2	cascade exit value
i	isentropic value
t	total condition

INTRODUCTION

Future vertical lift vehicles that can have both vertical takeoff and Mach 0.5 cruise capability will require enabling technologies such as variable speed power turbines (VSPT) or variable speed gears (Refs. 1, 2). While conventional methods for reducing turbine speed is through gearing, future aircraft may require up to 50% reduction in the main rotor speed during cruise. As a result of this change in rotor speed, the power turbine blades will see a large variation in incidence flow angle. Technologies using incident tolerant blading can optimize propulsive efficiency by allowing the power turbine to change shaft speed while minimizing weight and fuel consumption. A VSPT must overcome these large incidence flow angle variations at high work factors and low Reynolds numbers over a wide operational speed range.

Several studies have addressed some of the challenges that are relevant to variable speed turbines. Welch et al (Ref. 2) provided details of the VSPT technology and the follow up technology transitions. Johnson et al (Ref. 3) and Acree et al (Ref. 4) described the benefits and challenges of vertical lift and Mach 0.5 cruise capable rotary wing vehicles such as the Large Civil Tilt-Rotor (LCTR) concept vehicle. The LCTR was the reference vehicle used as the baseline for several aerodynamic

studies performed by NASA and Army Research Laboratory. Experimental studies have been reported in References 5-7 detailing 5-hole probe surveys at various flow rates and incidence angles, blade loading, and loss buckets. One area requiring further investigation is determining the location of transition from laminar to turbulent flows and where separation occurs in order to optimize future VSPT blade designs. Low turbulence experimental data on such blades can prove to be challenging test cases for computational fluid dynamics (CFD) code and model improvement.

The objective of the present study is to advance the understanding of the aerodynamic effects of large incidence angle and Reynolds number variations in order to address key VSPT challenges. Among those challenges is to improve the computational modeling of complicated flows such as those seen in a VSPT, with a wide range of incidence angles and flowrates. In the present study, flow separation and transition were measured using infrared imaging of a heated endwall surface of a linear cascade with variable speed power turbine blades. Since this is a low pressure turbine application, the heat transfer measurements in this study are not primarily meant for determining local hot areas needing cooling, but rather to use the technique as a method to visualize flow transition and separation on the endwall surface. A range of flowrates spanning orders of magnitude of the baseline flow condition were investigated at several incidence angles similar to studies described in References 5-7. The endwall data along with the blade surface heat transfer data currently being acquired will provide beneficial information for CFD code and turbulence model improvement and help optimize future incident tolerant blade designs.

DESCRIPTION OF EXPERIMENT

The heat transfer measurements on the endwall of the 2-D VSPT blade section were conducted in the Transonic Turbine Cascade Facility at NASA Glenn Research Center, and is shown in Figure 1. A description of the facility can be found in Reference 5. The cascade is comprised of nominally ten blades that represent a scaled 2-D midspan section of the VSPT second stage rotor, with geometry details described in Ref. 8 and summarized in Table 1. The cascade has the capability to test large scale models (span of 6 inches) with continuous flow at engine relevant Mach and Reynolds numbers. In addition, the cascade is attached to a wheel that can be rotated to provide incidence angles from +15.8° to -51°, as shown in Figure 2; this allows for a wide range of incidence angles to be studied. Table 2 lists the angles used in this effort. Inlet air is supplied by a 40 psig combustion air system, which provides clean dry ambient temperature air. The air is then passed through a flow conditioner and a contraction section, and then into the main test section with upper and lower flow boards, and exhausting through an altitude exhaust system maintained at 2 psia. For the current tests, no turbulence grid was installed, providing low turbulence intensities of 0.8%.

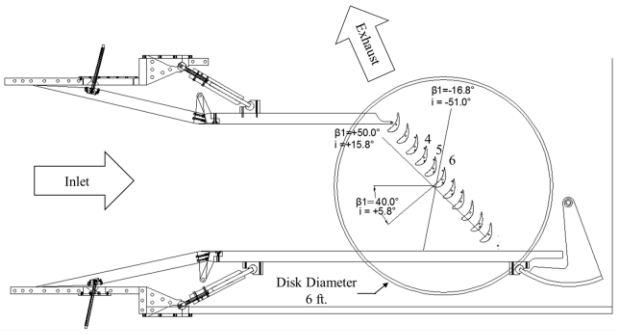

Figure 1. Transonic turbine blade cascade facility.

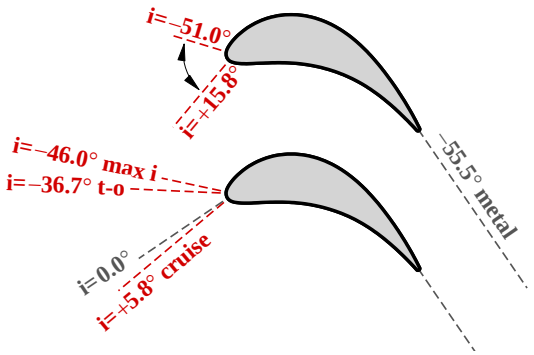

Figure 2. Incidence angles of VSPT blade

Table 1. Blade parameters

Axial Chord, C_x [inch]	7.109
True Chord [inch]	7.655
Pitch, S [inch]	5.119
Span, H [inch]	6.000
Solidity, C_x/S	1.389
Aspect Ratio, H/C_x	0.844
Throat Dimension [inch]	2.868
Stagger Angle [deg]	20.35°
Inlet Metal Angle [deg]	34.2°

Uncovered Turning [deg]	19.47°
Exit Metal Angle [deg]	−55.54°

Table 2. Inlet flow angles

Incidence Angle, i	Tunnel Inlet Angle, β_1	Zw
15.8°	50.0°	1.22
5.8° (cruise)	40.0°	1.06
–16.1°	18.1°	0.82
–36.7° (takeoff)	–2.5°	0.65
–46.0° (max mission)	–11.8°	0.58
–51.0°	–16.8°	0.53

Table 3. Nominal tunnel flow conditions

Case #	Exit Reynolds No., $Re_{Cx,2}$	Reynolds No. baseline factor	Pressure Ratio	Exit Mach No., $Ma_{2,i}$
1	0.212×10^6	0.4	1.087	0.35
2	0.530×10^6	1	1.087	0.35
3	0.530×10^6	1	1.412	0.72
4	1.060×10^6	2	1.412	0.72
5	2.120×10^6	4	1.412	0.72

Baseline Exit Reynolds number, $Re_{Cx,2,baseline}$=530,000.
Design Pressure Ratio = 1.412 → $M_{2,i}$ = 0.72.

At each incidence angle setting from Table 2, data was acquired at the five nominal flow conditions listed in Table 3. The design pressure ratio of 1.412 was used which corresponds to an exit isentropic Mach number $M_{2,i}$ of 0.72. A baseline flow condition, Re_b based on axial chord length, was determined by finding the lowest Reynolds number that the tunnel could maintain at an exit Mach number of 0.72, which was found to be 0.53×10^6. Since the lowest Reynolds number point of 2.12×10^5 could not be reached at the design exit Mach number due to limitations of the tunnel operating envelope, the Mach number for this case was reduced to 0.35. Additional overlap flow points were tested at $M_{2,i}$ of 0.35 and 0.72 at 1.0* Re_b. Nominal boundary layer thickness ranged from 1.6 inch at the lowest flowrate to 1.2 inch at the highest flowrate.

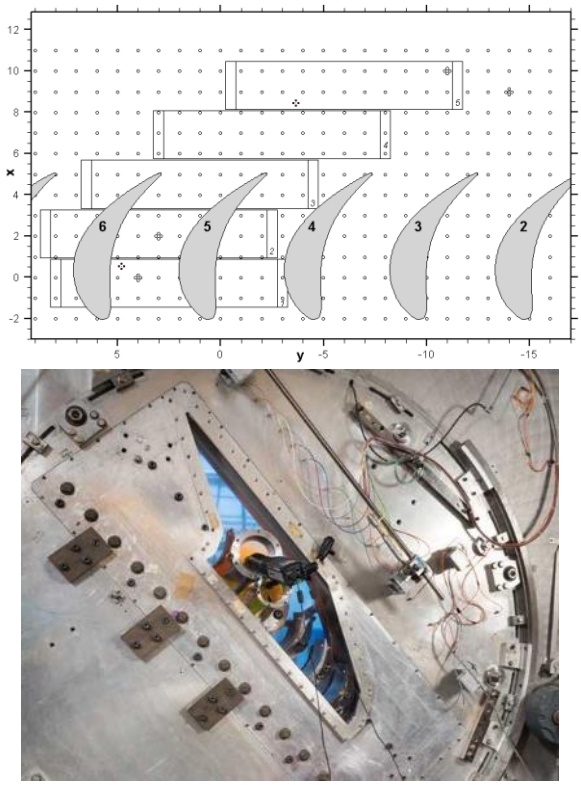

Figure 3. Endwall test section: a) heater strip locations; b) infrared window ports and cameras

The instrumented section of the endwall was a foam insert coated with a gelcoat that fit inside an aluminum outer wall. Five heater strips connected in series were attached to the foam endwall section spanning one of the passages between blades 5 and 6 in the cascade, as shown in Figure 3a. Inconel foil was attached to the surface with double sided tape, with the end of each strip tack welded to a copper bus bar. With the five heater strips connected in series, one end of heater strips 1 and 5 were connected to a power supply.

Heat flux was determined for each individual heater strip. Two thin film thermocouples were attached to the surface to provide a surface temperature for calibration of the infrared thermography images. Two FLIR infrared cameras were used to acquire temperatures on the endwall, with one camera viewing the upstream portion of the passage and one viewing the downstream portion of the passage through two coated ZnSe infrared viewing ports as shown in Figure 3b. The endwall was painted black to provide an emissivity of approximately 0.96, and grid dots spaced one inch apart were added to

the surface to assist in correcting any angled or distorted images.

Nusselt number values were determined by using the following equation:

$$Nu = hL/k = QL/A/k/dT,$$

in which Q is the heater strip heat flux, A is the total area of each heater strip, L is the axial chord length, and k is the thermal conductivity of the Inconel foil. The temperature difference dT is the difference between the surface temperature in the image with heat applied and the adiabatic surface temperature in an image with no heat applied. Since the images were taken at angles and the cameras were not completely perpendicular to the surface, the Nusselt images were run through a view correction program and converted to unwrapped Cartesian coordinates.

EXPERIMENTAL RESULTS

Measurements were taken on the instrumented endwall of the cascade at five flow conditions and six incidence angles. Two of the flow conditions were at a nominal exit Mach number $M_{2,i}$ of 0.35 and Reynolds numbers of $0.4*Re_b$ and $1.0*Re_b$, and three were at a nominal $M_{2,i}$ of 0.72 and Reynolds numbers of $1.0*Re_b$, $2.0*Re_b$, and $4.0*Re_b$. Incidence angles were i=15.3°, 5.3° (cruise), -16.1°, -36.7° (takeoff), -46.0°, and -51°.

Figure 4 shows a composite plot of Nusselt number for the five flow conditions at a blade incidence angle of +5.8°, cruise condition. Note that the scales are not the same and were chosen to bound the minimum and maximum Nusselt number for each flow condition. Also the high *Nu* regions near the leading edge of the first heater strip and on the edges of each the downstream heater strips are a result of the adjacent unheated surfaces. As expected, heat transfer increases with increasing Reynolds number, and secondary flow features are evident. Comparing flow conditions 2 and 3, which have the same Reynolds number of $1.0*Re_b$ but different $M_{2,i}$, the Nusselt contours appear to be similar, with a low *Nu* region near the center of the passage. This is not surprising given that Nusselt number is a stronger function of Reynolds number than of Mach number. As flowrate increases, this low *Nu* region diminishes; *Nu* increases as turbulent flow begins to increase in the passage. In addition, the wake behind the trailing edge of the blade appears to be shifted toward the suction side of the passage. A low Nusselt number region can be seen near the downstream of the suction side of the blade, possibly indicating separated flow. This corresponds with the secondary flow pattern seen in the previously acquired pressure survey data from Ref. 5. Figure 6 shows the pitchwise total pressure coefficients at 7% axial chord distance downstream of the trailing edge of the blade, with y representing the pitchwise direction and z representing the spanwise direction. The small corner vortex seen near the endwall agrees with the location of the wake in the heat transfer data.

Figure 5 shows composite plots at the takeoff blade incidence angle of -36.7°. Again these plots are not on the same scale and are bounded by the minimum and maximum Nusselt number for each flow condition, and the high *Nu* regions near the leading edge of the first heater strip and on the edges of each the downstream heater strips are a result of the adjacent unheated surfaces. The flow pattern through the passage has changed relative to that seen at the cruise incidence angle, however there still appears to be a slight separation region near the downstream of the suction side similar to the cruise angle. This is also seen in the pressure survey data shown in Figure 6. A higher *Nu* wake can be seen directly behind the blade trailing edge, with a shifted low *Nu* region further downstream. This again corresponds with the secondary flow pattern seen in the previously acquired pressure survey data in Figure 6. The passage vortex emanating from the horseshoe vortex shedding off the leading edge of the blade can be seen in the streak of low Nu across the middle of the passage. Flow conditions 2 and 3 are again similar to each other, with a small high *Nu* region near the middle of the suction side forming in the accelerating region of the passage. This accelerating region increases with increasing Reynolds number.

The six incidence angles at the flow condition $4.0*Re_b$ are shown in Figure 7. The other flow conditions showed similar trends and are not included here for brevity. Starting with i=15.8°, the separation region on the suction side can be seen to get smaller as incidence angle decreases. In addition, the pressure side starts to see what appears to be separation near the leading edge with the most negative incidence angles. This separation and the ensuing reattachment leads to turbulent boundary layer on the pressure side thus enhancing the heat transfer rate. Relatively high heat transfer rates are present on the near trailing edge portion of the pressure side for the negative incidences are most likely due to transition and not caused by reattachment.

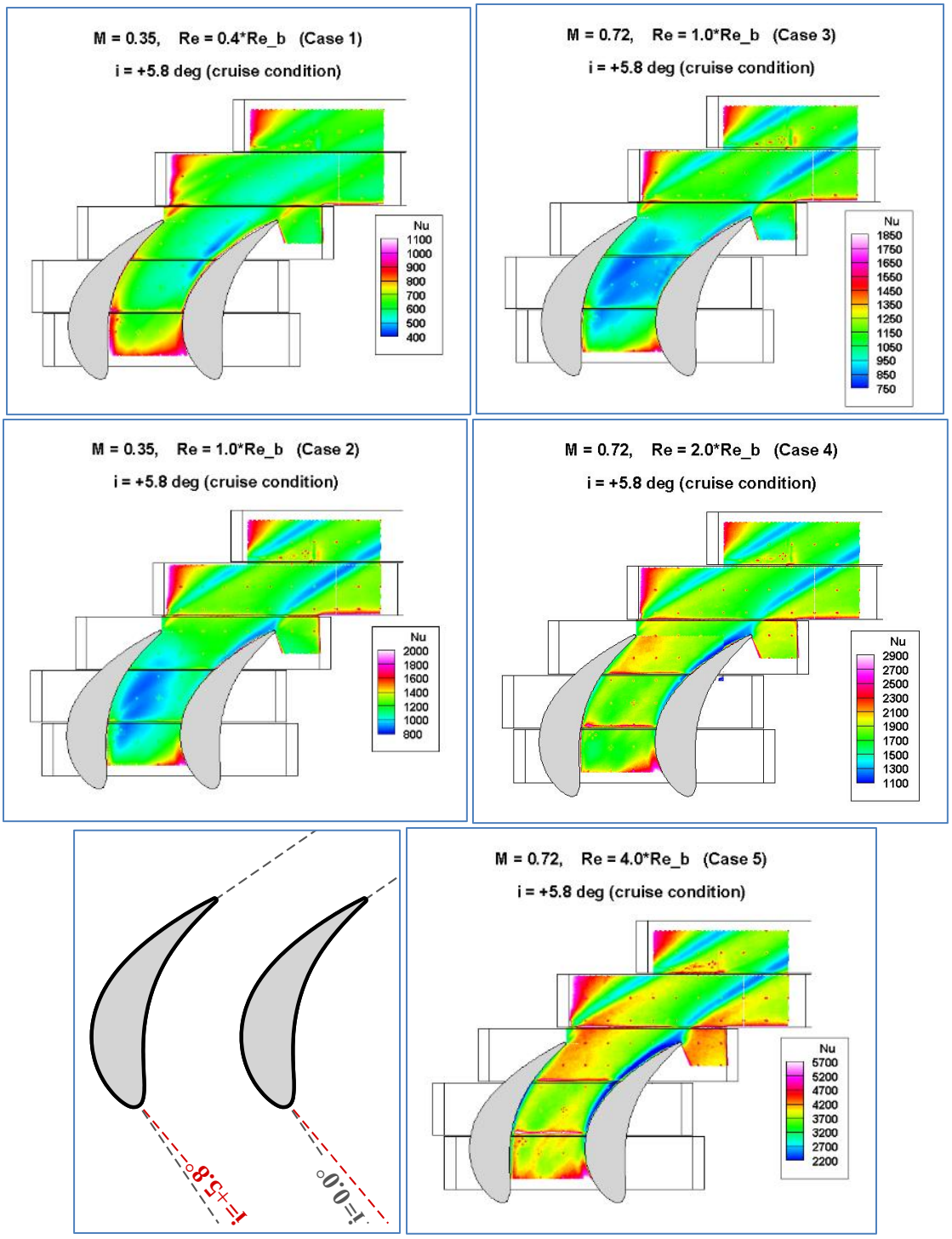

Figure 4. Endwall Nusselt number at cruise, *i* = +5.8°

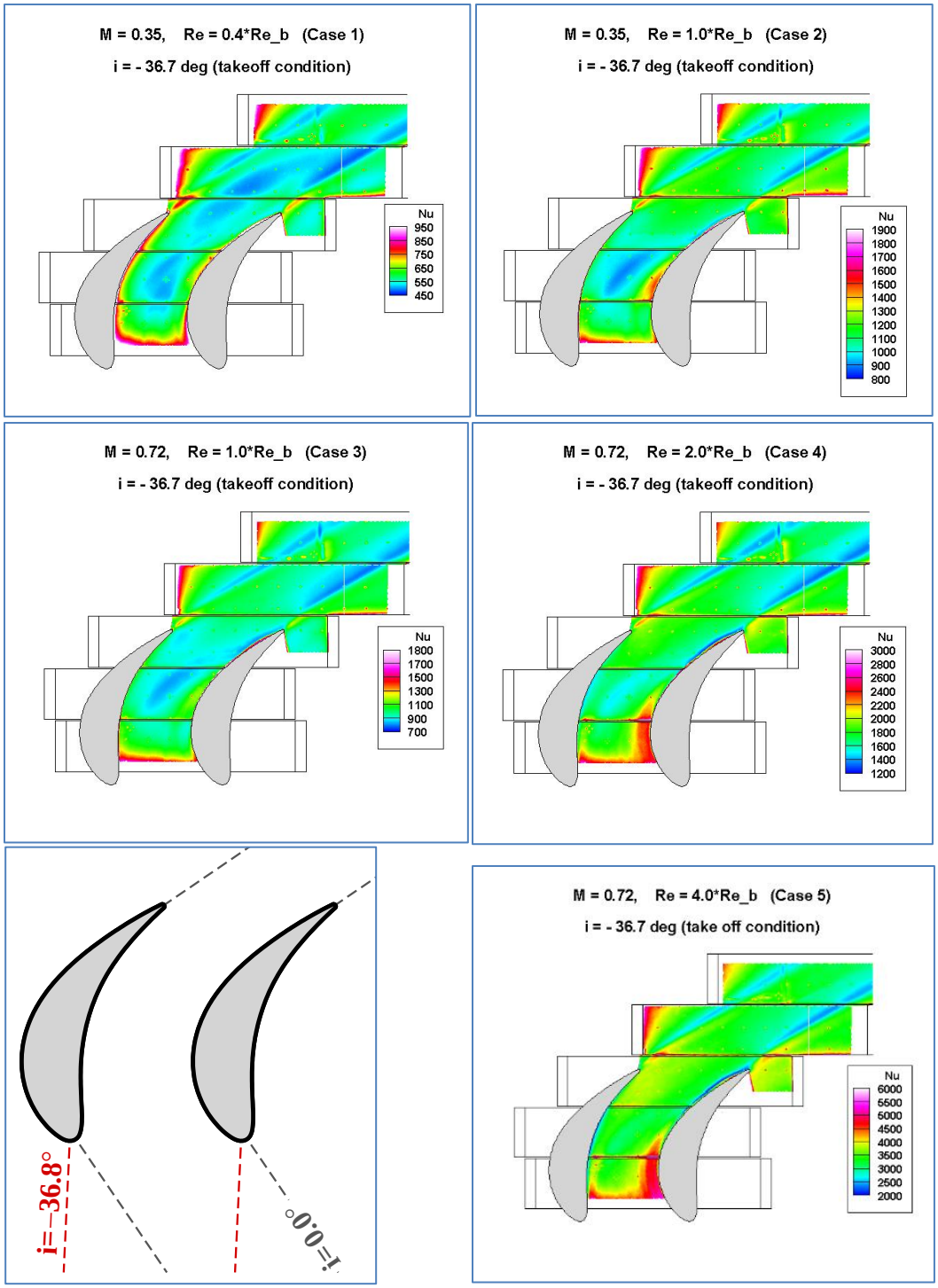

Figure 5. Endwall Nusselt number at takeoff, *i* = -36.7°

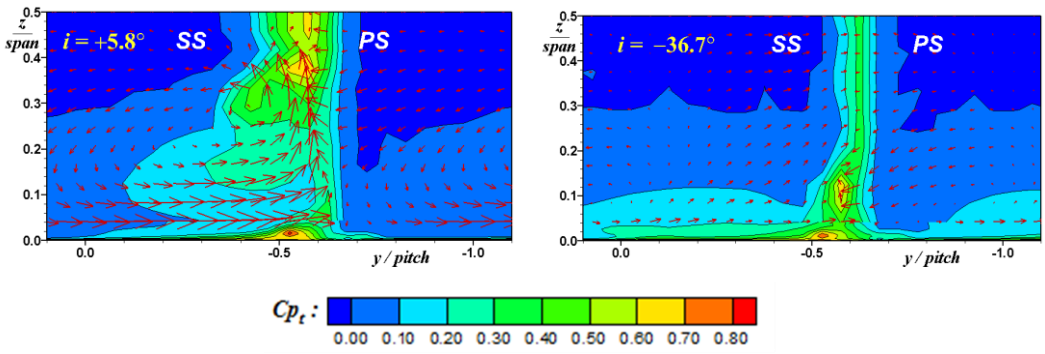

Figure 6. Total pressure coefficient contours and secondary flow vectors over one blade passage downstream of blade (Ref. 5)

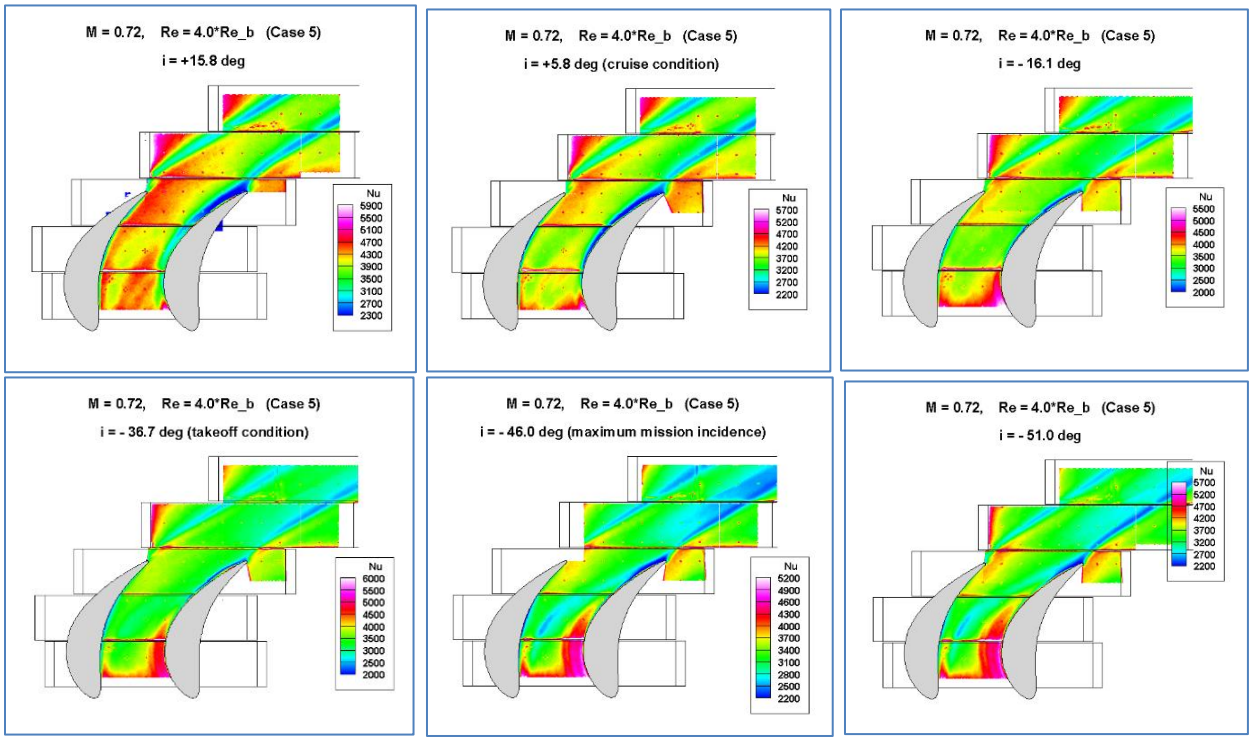

Figure 7. Endwall Nusselt number at 4.0*Re_b

Flow transition was also investigated by comparing the Nusselt-Reynolds number correlation values for the different flow conditions, where $Nu = A*Re^B$. While this correlation is intended for flow over a flat plate, it is still useful in determining where flow transitions from laminar to turbulent on the endwall. Plotting local *B* values calculated from multiple flow conditions gives an indication of the state of the local boundary layer as the flow transitions from one condition to another. For a flat plate, a value for *B* of 0.5 indicates laminar flow, and a value of 0.8 indicates turbulent flow. Guzovic (Ref. 9) determined a generalized statistical correlation for a cascade endwall for flow conditions ranging from laminar through turbulent, yielding *A*=0.0837 and *B*=0.7494. The current data from all flow cases at each incident angle was fit to this form. The coefficient A was forced to 0.0837, and B was determined by a least squares data fit, and are shown in Figure 8. The results show exponent values that match Guzovic's correlation fairly well with exponent values near 0.73. The higher Reynolds number cases are expected to be mostly turbulent, and Figure 8 generally indicates a mostly

turbulent flow situation. There may be some indication of laminar or possibly separated flow near the suction side trailing edge corner vortex region where the darker areas of lower *B* are located, as well as the passage vortex at the more negative incidence angles. This is also similar to what was seen in the Nusselt plots in Figure 7.

Alternatively, the correlation can be limited to Nu data from just two Reynolds number cases and evaluated whether any regions of laminar flow are evident. A ratio of the Nusselt correlation based on two flow conditions can be used to determine the exponent *B*:

$$\frac{Nu_2}{Nu_1} = \left(\frac{Re_2}{Re_1}\right)^B$$

Figures 9a and 9c shows the values of the exponent *B* for the ratios of case 1 (*M*=0.35 and *Re*=0.4**Re*$_b$) and case 2 (*M*=0.35 and *Re*=1.0**Reb*) for the cruise angle. Similarly Figures 9b and 9d show the values of *B* for the ratios of case 3 (*M*=0.72 and *Re*=1.0**Re*$_b$) and case 5 (*M*=0.72 and *Re*=4.0**Re*$_b$) at the takeoff angle. Figure 9a seems to show areas of laminar flow transitioning to turbulent flow. The inlet boundary layer is fully turbulent, so it is possible that at lower Reynolds numbers, the acceleration through the passage re-laminarized the flow, especially near the pressure surface. Additionally, lower *B* values can be seen near the suction side downstream corner vortex region. The exponent values of greater than 0.8 in Figure 9b seem to indicate a turbulent flow throughout most of the endwall passage, with the exception near the wall suction side trailing edge. The mid region with *B* values as high as 1.25 is much greater than the typical turbulent flat plate values of 0.8; this is most likely due to the strong secondary flows in the passage. Figures 9c and 9d show similar results for the case1/case2 and case3/case5 correlations at the takeoff angle. Changing incidence angle affects the main and secondary flow features, and thus the general shape of the endwall heat transfer is different. Similar to the lower Reynolds number cases at cruise angle, there are regions of lower heat transfer (lower values of *B*) which would indicate laminar flow. The higher Reynolds cases again indicate a more turbulent flow, with a few regions of very high heat transfer where high acceleration occurs along the suction surface. Additionally the trailing edge suction side still shows some signs of laminar flow.

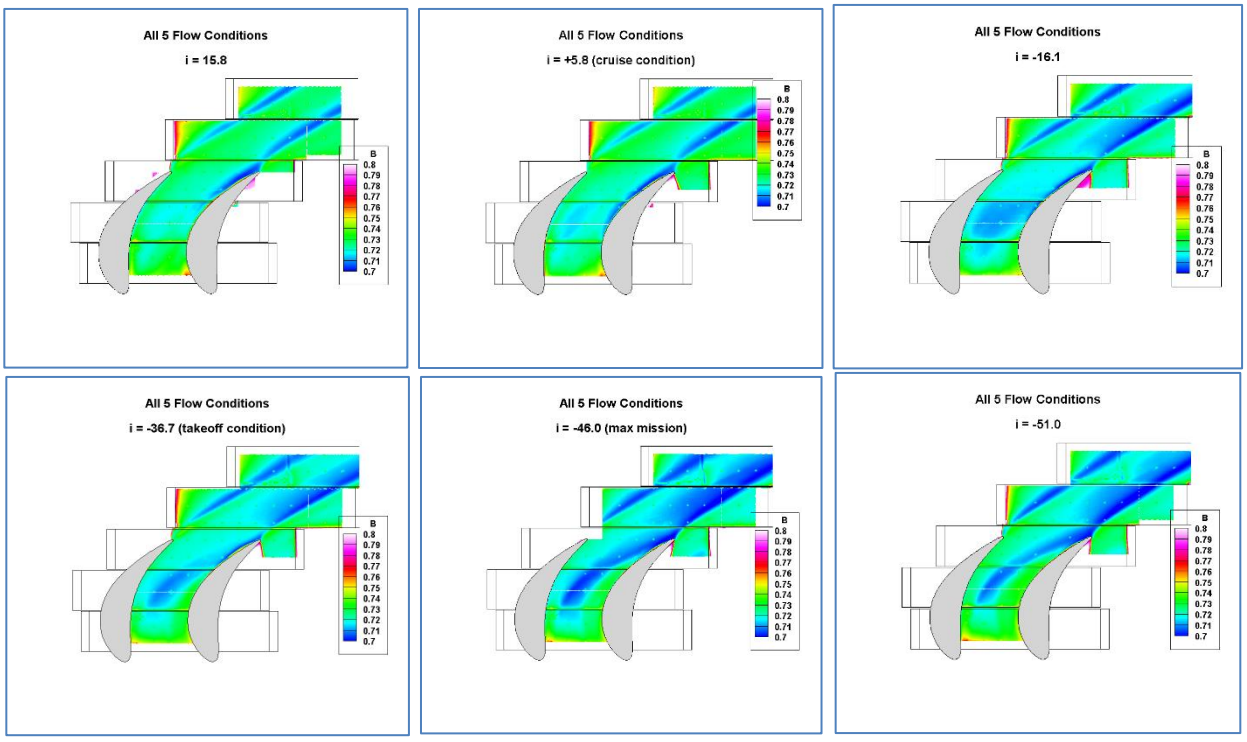

Figure 8. Values of the exponent B of the Nusselt-Reynolds correlation Nu = 0.837*Re^B

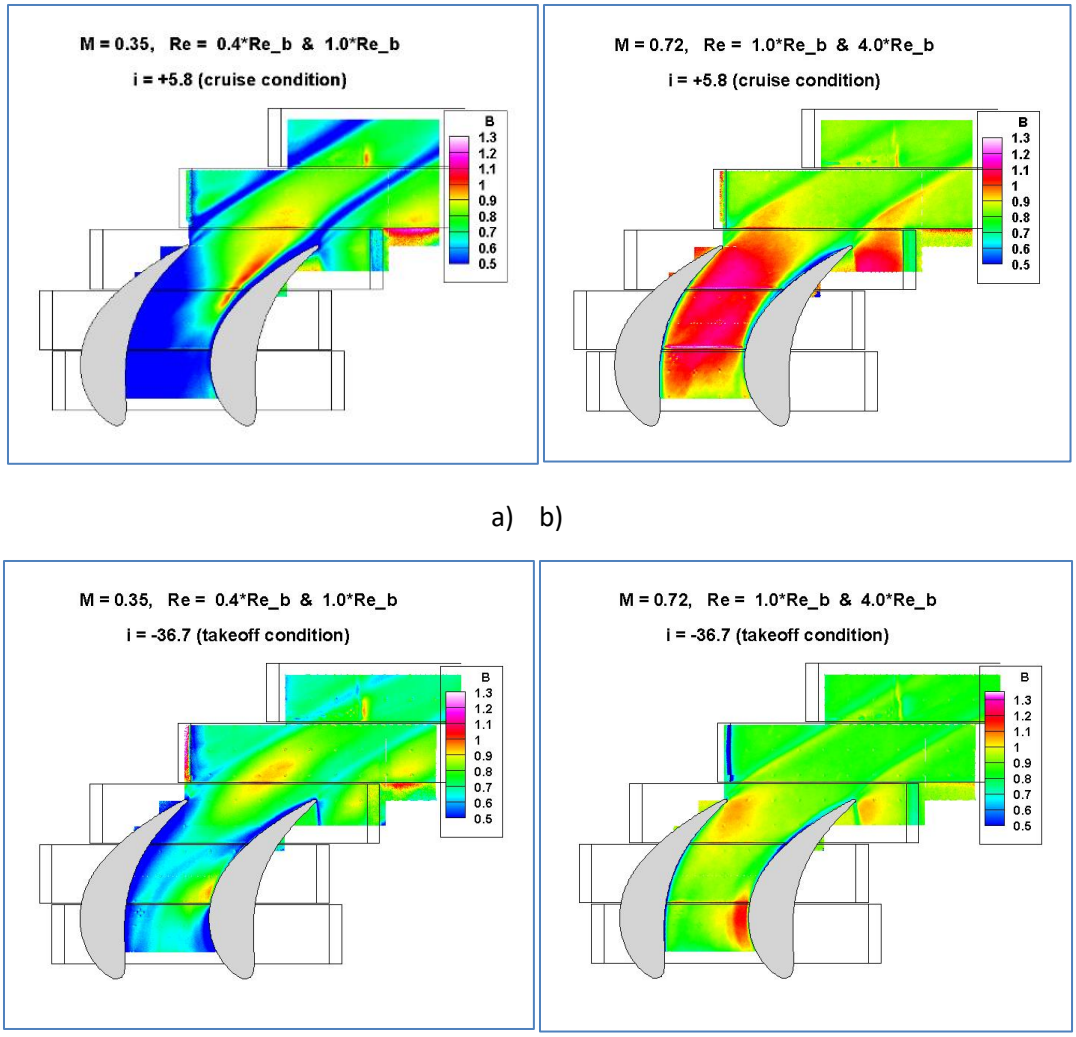

Figure 9. Values of the exponent B from ratio of Nusselt correlations

CONCLUSIONS

The effects of flow transition and separation were investigated over large variations in incidence angle and Reynolds number using infrared thermography on the endwall of a VSPT cascade at low turbulence intensity. Heat transfer measurements on the endwall were acquired for several incidence angles and flowrates, showing regions where separated flow occurred along the blade surface. A Nusselt-Reynolds number correlation provided insight for where transition from laminar to turbulent flow may occur along the passage between blades. Additional heat transfer tests are currently being investigated on the surface of an instrumented blade to complement the endwall data presented in this study.

Author contact:

Douglas Thurman drthurman@nasa.gov
Philip Poinsatte poinsatte@nasa.gov
Paul Giel paul.w.giel@nasa.gov
Barbara Lucci lucci@nasa.gov

REFERENCES

1. D′Angelo, M., “Wide Speed Range Turboshaft Study,” NASA CR-198380, Aug. 1995.

2. Welch, G.E., “Assessment of Aerodynamic Challenges of a Variable-Speed Power Turbine for Large Civil Tilt-Rotor Application,” Proc. AHS Int. 66th Annual Forum, May, 2010; also NASA/TM—2010-216758, Aug. 2010.

3. Johnson, W., Yamauchi, G. K., and Watts, M.E., "NASA Heavy Lift Rotorcraft Systems Investigation,"NASA/TP—2005-213467, Sep. 2005.

4. Acree, C.W., Hyeonsoo, Y., and Sinsay, J.D., "Performance Optimization of the NASA Large Civil Tiltrotor," Proc. Int. Powered Lift Conf., London, UK, Jul. 22-24, 2008.

5. Flegal-McVetta, A., Giel, P., Welch, G., "Aerodynamic Measurements of a Variable-Speed Power-Turbine Blade Section in a Transonic Turbine Cascade at Low Inlet Turbulence," NASA/TM—2013-218069.

6. Flegal, A., Giel, P., Welch, G., "Aerodynamic Effects of High Turbulence Intensity on a Variable-Speed Power-Turbine Blade with Large Incidence and Reynolds Number Variations," AIAA 2014-3933.

7. Flegal, A., Giel, P., Ames, F., Long, J., "Complementary Aerodynamic Performance Datasets for a Variable Speed Power Turbine Blade Section from Two Independent Transonic Turbine Cascades," ISABE2015-20163.

8. Ford, A, Bloxham, M., Turner, E., Clemens, E. and Gegg, S., "Design Optimization of Incidence-Tolerant Blading Relevant to Large Civil Tilt-Rotor Power Turbine Applications," NASA/CR—2012-217016, Dec. 2012.

9. Guzovic, Z., Matijasevic, B., Rusevljan, M., "Generalized Correlations For Heat Transfer Determination In Turbine Cascades," Journal of Mechanical Engineering, Vol. 47, No. 8, 2001.